REDVET - Revista electrónica de Veterinaria - ISSN 1695-7504
Vol 25, No. 2 (2024)
http://www.veterinaria.org
Article Recieved: 16/09/2024, Revised: 18/10/2024, Accepted: 09/12/2024

Green synthesis, Characterization and Anticancer activityof Clerodendrum infortunatum mediated ZrO_2 and Ag doped ZrO_2 nanoparticles

H. R. Uma[1] and Jessica Fernando[2]

[1.] Research Scholar (Register No: 20113112032013) Department of Chemistry, V. O. Chidambaram College, Thoothukudi - 628 008, Affiliated to Manonmaniam Sundaranar University, Abishekapatti - 627 012, Tamil Nadu, India, Tamil Nadu, India Email: umahrchem@gmail.com
[2.] Associate Professor, Department of Chemistry, V. O. Chidambaram College, Thoothukudi - 628 008, Affiliated to Manonmaniam Sundaranar University, Abishekapatti - 627 012, Tamil Nadu, India, Tamil Nadu, India Email: jessivoc@yahoo.com

Abstract
Clerodendrum infortunatum extract was employed for the green synthesis of pure ZrO_2 and Ag-doped ZrO_2 nanoparticles. The study aimed to evaluate their anticancer efficacy against AGS (human gastric adenocarcinoma) cells. The nanoparticles were characterized by XRD, EDS, TEM, XPS, UV-visible spectroscopy, and photoluminescence. Cytotoxicity assays (MTT) on AGS cells showed that both pure ZrO_2 and Ag-doped ZrO_2, as well as the plant extract alone, induced cell death, with the doped sample exhibiting significantly stronger activity. Consequently, the biogenic nanoparticles qualify as promising anticancer agents for biomedical applications.

Keywords: Green synthesis; Nanoparticles; Clerodendrum infortunatum leaves; Anticancer activity; Cell viability

1. Introduction

In recent years, the general public has encountered a range of health challenges, the most critical being resistance of cancer cells to therapy. Bacterial infections cause numerous problems—disease, mortality, and organ malformations—that are typically managed with antibiotics [1, 2]. However, the extensive use of antibiotics not only eliminates beneficial microbes but also leads to systemic side effects such as neurological suppression, prompting researchers to devise innovative approaches that curb harmful resistance and spread [3]. Nanoscale materials consistently provide the scientific community with novel and potent antibacterial solutions. Biogenic nanoparticles have shown enhanced activity against a broad spectrum of bacterial strains, helping to overcome resistance issues [4]. Meanwhile, cancer— a condition in which the body's own defense system fails to eliminate malignant cells—has been a major cause of morbidity and mortality over recent decades. The major obstacles to optimal cancer treatment are the systemic cytotoxicity and severe side-effects associated with radiotherapy, limiting therapeutic effectiveness [5]. Furthermore, chemotherapy agents are poorly selective; they kill many healthy cells, suppress the immune system, and often lead to drug resistance [6]. The rise of nanoscience and nanotechnology now offers countless technical and industrial possibilities for manipulating matter at the nanoscale. Metal oxides—including ZnO [2], CuO [3], ZrO_2 [7], SnO_2 [8], TiO_2 [9], etc.—act as effective antimicrobial agents because of their high efficiency, abundant reactive - oxygen species, low cost, simple synthesis routes, strong optical band gaps, and large surface - to - volume ratios. Among these candidates, zirconium oxide (ZrO_2) stands out for its thermal stability, chemical inertness, and mechanical robustness, making it highly promising for future applications. ZrO_2 is employed in biomedical imaging, materials science, synthesis of inorganic compounds, optics, electronics, and biological fields [10-13], as well as in photodynamic therapy. Moreover, doping ZrO_2 with transition metals can tailor its properties, enhancing its functionality for specific uses. Among transition metals, silver (Ag) is especially significant because it can fine-tune the optical characteristics of ZrO_2 nanomaterials [14]. Silver, a transition metal with high electrical and thermal conductivity, has a long history of medical use, though its fundamental antimicrobial action was recognized later. Today, biosynthesis of nanoparticles offers a cheap, eco-friendly substitute for chemical and physical routes. Plant-mediated nanoparticle synthesis represents a green-chemistry approach that links nanotechnology directly with botanical resources [15]. The green synthesis of nanostructures offers an environmentally benign solution for agriculture, biomedicine, and remediation of polluted sites [16]. This method exploits secondary metabolites present in any plant part [17]. Kumar et al. [18] described the phyto-mediated preparation of ZnO nanoparticles from Clerodendrum infortunatum leaf extract and demonstrated enhanced antibacterial activity. To date, no study has reported the incorporation of dopants into ZrO_2 using Clerodendrum infortunatum leaf extract. Here, we present the green synthesis of pure ZrO_2 and Ag-doped ZrO_2 nanoparticles with the same leaf extract. The products were characterized by XRD, TEM, EDS, XPS, UV-visible spectroscopy, and photoluminescence. Anticancer activity was assessed via MTT assays.

Materials and methods

1.1 Materials

The chemicals employed were Zirconyl nitrate ($ZrO(NO_3)_2.xH_2O$) and silver nitrate ($AgNO_3$), obtained from SRL Chemicals at 99 % purity. All reagents were analytical-grade and used as received without further purification. Aqueous solutions were prepared with double-distilled water.

REDVET - Revista electrónica de Veterinaria - ISSN 1695-7504
Vol 25, No. 2 (2024)
http://www.veterinaria.org
Article Recieved: 16/09/2024, Revised: 18/10/2024, Accepted: 09/12/2024

1.2 Preparation of leaf Extract

Clerodendrum infortunatum leaves were harvested, rinsed with tap water and then repeatedly with double-distilled water, and dried. 30 g of leaves were added to 150 mL of double-distilled water and heated to 80 °C, yielding a yellow-coloured solution. After cooling to room temperature, the extract was filtered through Whatman paper and stored in a refrigerator for later use.

1.3 Synthesis of pure ZrO_2 nanoparticles

5 g of $(ZrO(NO_3)_2.xH_2O)$ was dissolved in 50 mL of double-distilled water. 10 mL of leaf extract was added with continuous stirring, and NaOH was introduced to reach pH 9. The mixture was stirred for 2 h, yielding a precipitate. After allowing the precipitate to settle for 24 h, it was filtered, washed with double-distilled water and ethanol, dried, and calcined at 500 °C for 2 h for further characterization.

1.4 Synthesis of silver doped ZrO_2 nanoparticles

5 g of $(ZrO(NO_3)_2.xH_2O)$ and 0.5 g of $AgNO_3$ were dissolved in 50 mL double-distilled water. 10 mL of leaf extract was added with continuous stirring, and NaOH was introduced to reach pH 9. The mixture was stirred for 2 h, yielding a precipitate. After allowing the solid to settle for 24 h, it was filtered, washed with double-distilled water and ethanol, dried, and calcined at 500 °C for 2 h for further characterization.

1.5 Characterization section

The crystal structure, phase identification and average crystallite size of the synthesized samples were examined by X-ray diffraction (XRD, PANalytical X'Pert Pro; Cu Kα, λ = 1.5406 Å, 40 kV, 30 mA). Transmission electron microscopy (TEM, JEOL JEM-2100F, 200 kV) provided high-resolution micrographs of the nanoparticles. X-ray photoelectron spectroscopy (XPS, PHI 5000 Versa Probe III) with a 0–5 keV Ar^+ ion gun (and optional 10/20 kV C_{60} gun) was used to analyse the Y 3d, O 1s and Ag 3d peaks. UV-visible absorption spectra were recorded at room temperature on a Perkin Elmer Lambda 35 spectrophotometer. Photoluminescence (PL) spectra were collected using a Cary Eclipse spectrophotometer at room temperature.

2.5.1 Anticancer activity

The human gastric adenocarcinoma (AGS) cell line, sourced from NCCS Pune, was maintained in DMEM/F12 medium with 10 % FBS and 1 % antibiotic-antimycotic solution at 37 °C, 5 % CO_2, and ~18–20 % O_2, with sub-culture every 2 days (passage 37 used). For the assay, 200 µL of cell suspension containing ~10 000 cells per well was seeded in a 96-well plate and incubated for 24 h, after which the test compounds (diluted in complete medium) were added and the plate was incubated for another 24 h under the same conditions. After the incubation period, the plates are removed from the incubator, the spent medium is discarded, and MTT reagent is added to achieve a final concentration of 0.5 mg ml^{-1}. The plate is wrapped in aluminium foil and returned to the incubator for exactly 3 h (incubation time may vary by cell line but must stay constant within the experiment). Next, the MTT solution is aspirated, 100 µL of DMSO (or other solubilisation solution) is added, and the mixture is gently shaken until the formazan crystals dissolve completely (pipetting may be needed for dense cultures). Absorbance is then measured at 570 nm using a spectrophotometer or ELISA reader, and cell viability (%) is calculated accordingly.

$$\text{Cell Viability (\%)} = \frac{\text{OD sample mean}}{\text{OD control mean}} \times 100\ \%$$

3. Results and Discussion

3.1. XRD analysis

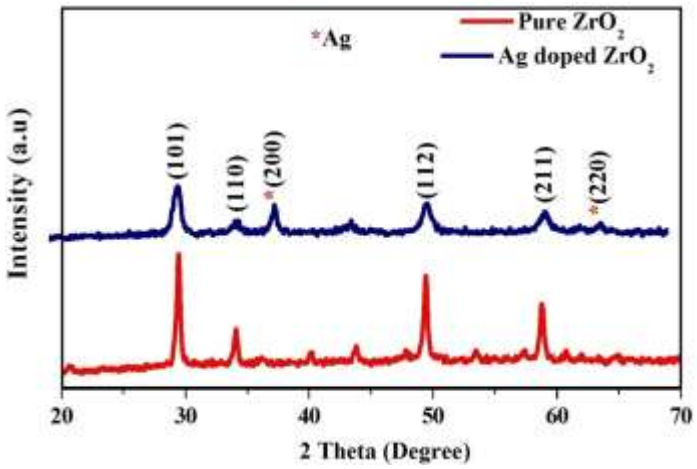

Fig. 1 XRD spectra of pure ZrO_2 and Ag doped ZrO_2 nanoparticles

REDVET - Revista electrónica de Veterinaria - ISSN 1695-7504
Vol 25, No. 2 (2024)
http://www.veterinaria.org
Article Recieved: 16/09/2024, Revised: 18/10/2024, Accepted: 09/12/2024

The pure ZrO_2 and Ag-doped ZrO_2 nanoparticles were identified from the XRD patterns shown in Fig. 1. The ZrO_2 diffraction peaks appear at $2\theta \approx 29.34°, 34.14°, 49.42°$ and $59.50°$, corresponding to the tetragonal planes (101), (110), (112) and (211) (JCPDS 68-0200) [19]. Additional peaks at 38.29° and 64.37° belong to the cubic silver phase $AgO_{(1-x)}$, indexed as (200) and (220), while the cubic Ag peaks match JCPDS 04-0783 [20]. This suggests that silver ions gradually migrated from the tetragonal ZrO_2 bulk to the surface [19]. Applying the Williamson-Hall (W-H) method, the peak broadening was deconvoluted into size and strain contributions using the standard relation [21].

$$\beta \cos\theta = \varepsilon\,(4\sin\theta) + \left(\frac{K\lambda}{D}\right) \text{---------- (1)}$$

Here, $\lambda = 1.5406$ Å is the X-ray wavelength, ε is the average microstrain, θ is the Bragg angle, $k \approx 0.94$ is the shape factor, and β is the full-width at half-maximum (radians). Fig. 2 shows the lattice strain extracted from the slope of the W-H plot for pure ZrO_2 and Ag-doped ZrO_2. From this analysis, the average crystallite sizes are ≈ 22.21 nm (pure) and ≈ 24.15 nm (Ag-doped). The dislocation density (δ) can then be calculated using Williamson and Smallman's formula [22].

$$\delta = \frac{1}{D^2} \text{---------- (2)}$$

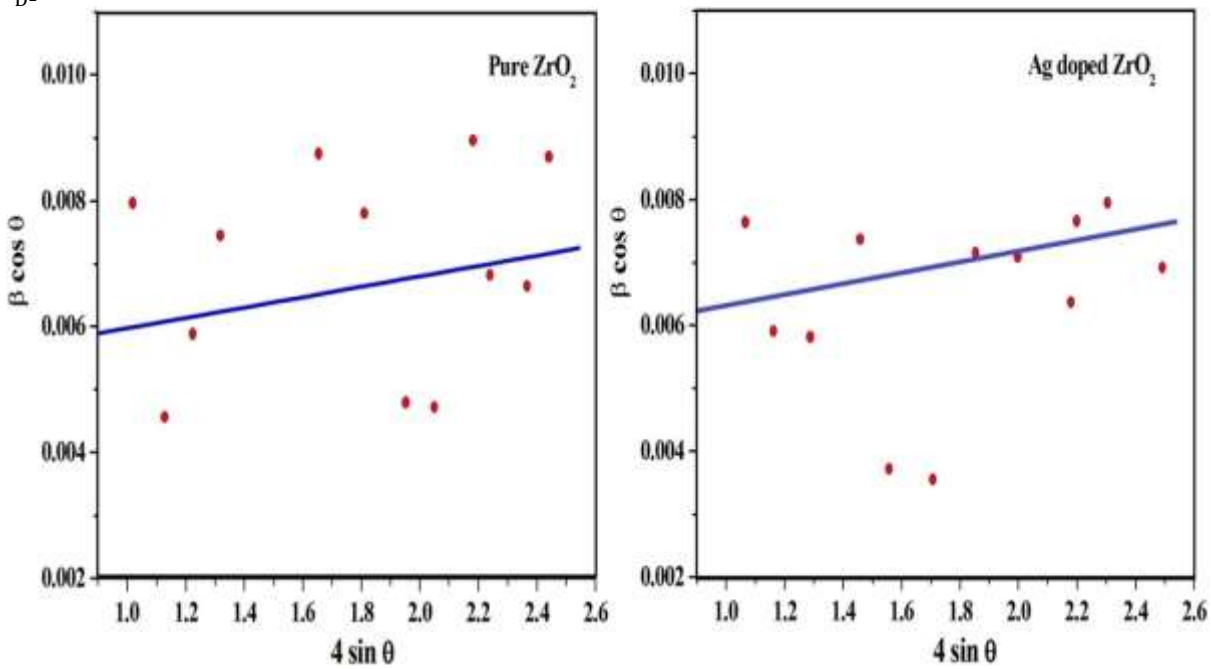

Fig. 2 W-H plot for pure ZrO_2 and Ag doped ZrO_2 nanoparticles

The calculated particle size, strain (ε) and dislocation density (δ) are listed in Table 1. Ag-doped ZrO_2 shows a lower dislocation density (1.71×10^{-3} nm^{-2}) than pure ZrO_2 (2.03×10^{-3} nm^{-2}), while pure ZrO_2 exhibits a slightly lower strain (7.43×10^{-4}) compared with Ag-doped ZrO_2 (8.31×10^{-4}). The δ values reflect the extent of crystal defects in each sample [23].

Table 1 XRD parameters of pure ZrO_2 and Ag doped ZrO_2 nanoparticles

	Williamsons Hall method		
Sample	Average Crystallite size D (nm)	Strain $\varepsilon \times 10^{-4}$	Dislocation density $\delta \times 10^{-3}$ nm^{-2}
Pure ZrO_2	22.21	7.43	2.03
Ag doped ZrO_2	24.15	8.31	1.71

REDVET - Revista electrónica de Veterinaria - ISSN 1695-7504
Vol 25, No. 2 (2024)
http://www.veterinaria.org
Article Recieved: 16/09/2024, Revised: 18/10/2024, Accepted: 09/12/2024

3.2 TEM and EDS analyses

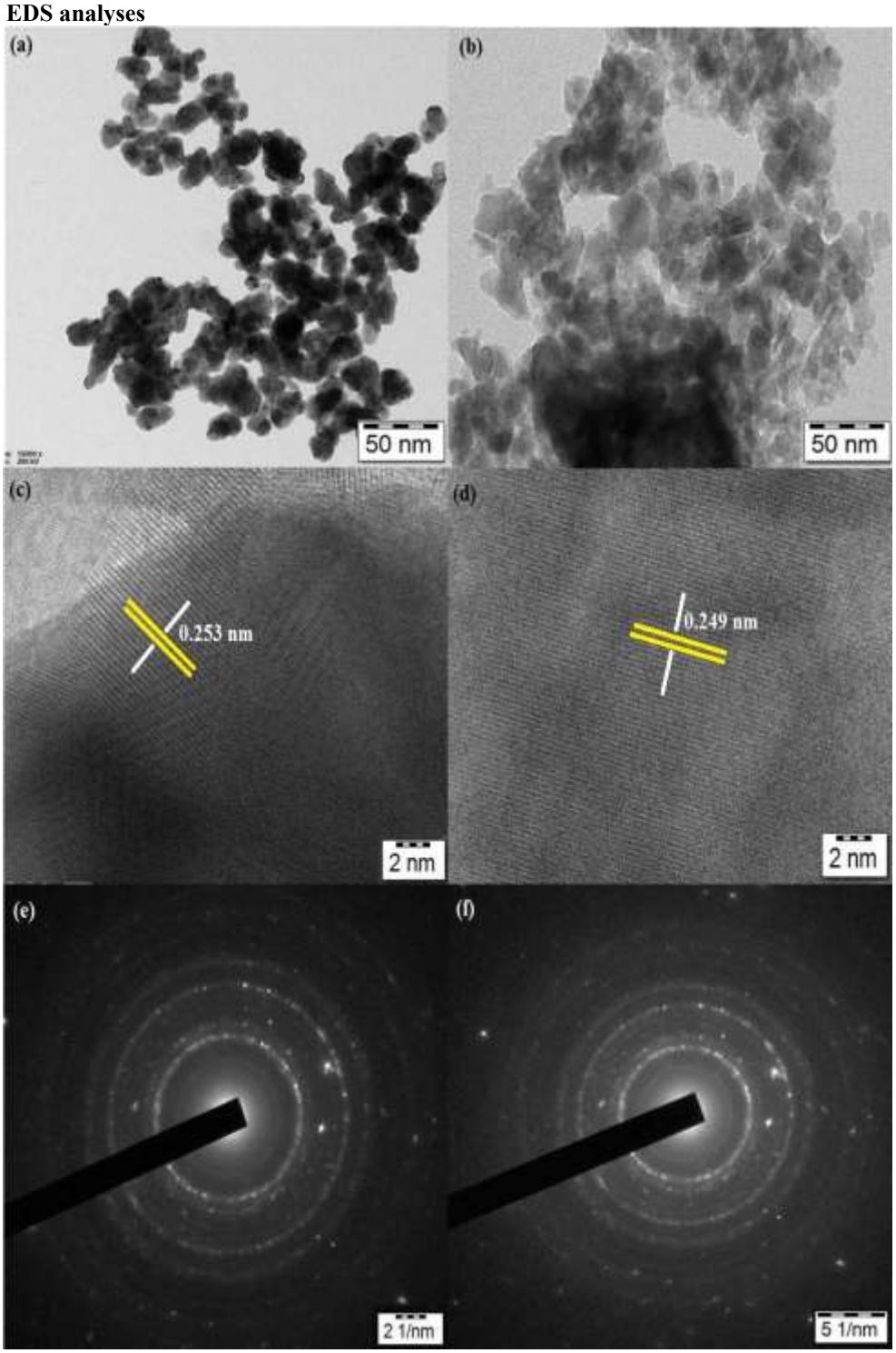

Fig. 3 (a and b) TEM image, (c and d) HRTEM image and SAED (e and f) of pure ZrO_2 and Ag doped ZrO_2 nanoparticles

The as-synthesized nanopowders were examined by TEM (Fig. 3a–b). Pure ZrO_2 and Ag-doped ZrO_2 appear irregular-to-spherical, with the doped particles measuring ≈ 25.23 nm (length) × 27.14 nm (width). HR-TEM revealed lattice spacings of 0.253 nm (pure) and 0.249 nm (Ag-doped), matching the (101) plane reported in the literature [24]. SAED patterns (Fig. 3c–f) display distinct diffraction rings consistent with the face-centered cubic structure and corroborate the XRD data. EDS spectra (Fig. 4) confirm the presence of only Zr and O in pure ZrO_2 (Fig. 4a) and the additional Ag peak in Ag-doped ZrO_2 (Fig. 4b), verifying sample purity and successful silver incorporation.

REDVET - Revista electrónica de Veterinaria - ISSN 1695-7504
Vol 25, No. 2 (2024)
http://www.veterinaria.org
Article Recieved: 16/09/2024, Revised: 18/10/2024, Accepted: 09/12/2024

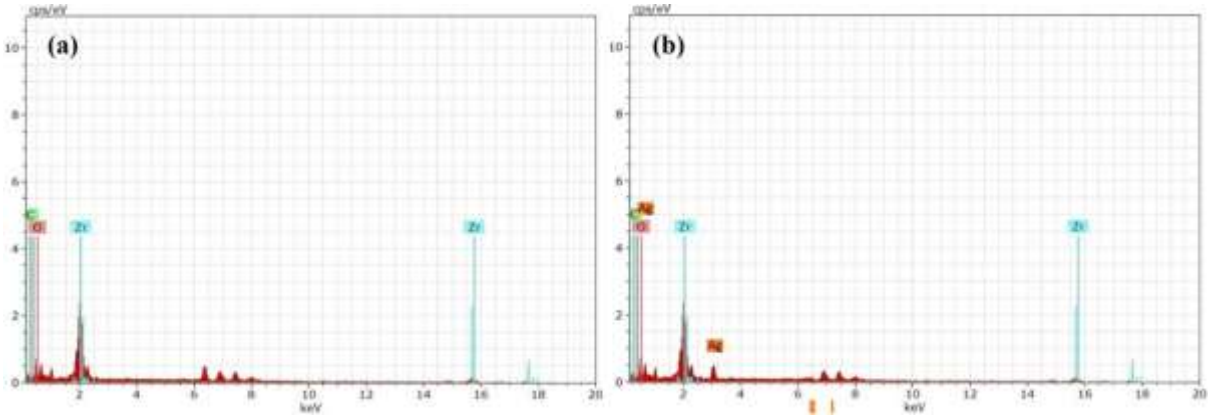

Fig. 4 EDS spectra of (a) pure $ZrO_2$and(b) Ag doped ZrO_2 nanoparticles

3.3 XPS spectra

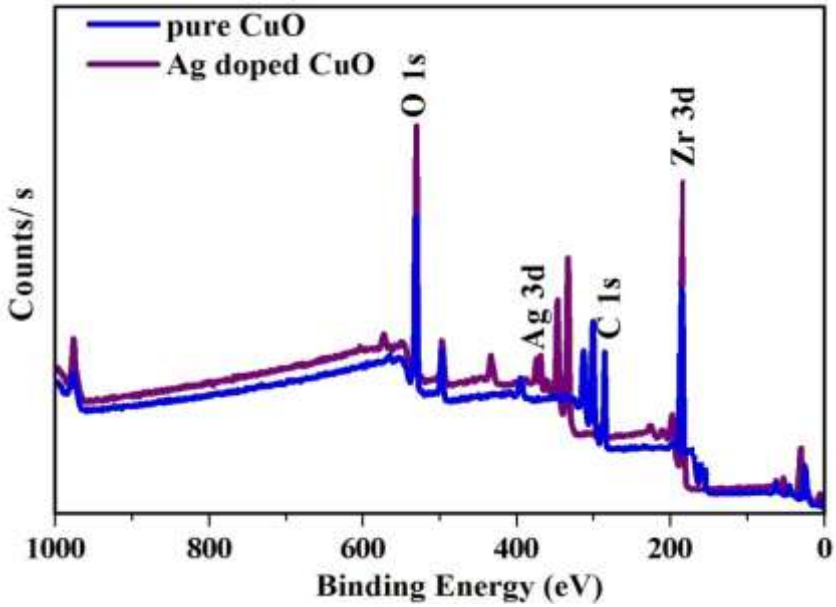

Fig. 4 X-ray photoemission survey spectra of pure ZrO_2 and Ag doped ZrO_2 nanoparticles

X-ray photoelectron spectroscopy (XPS) was performed to probe the surface elemental composition and oxidation states of pure ZrO_2 and Ag-doped ZrO_2 nanoparticles. The survey spectrum of the Ag-doped sample (Fig. 4) exhibits distinct C 1s, O 1s, Zr 3d and Ag 3d peaks, confirming the presence of these four elements and matching the EDS results. All binding energies were referenced to the adventitious C 1s signal set at 282.88 eV, which arises from atmospheric carbon contamination [25]. The high-resolution Zr 3d XPS spectrum (Fig. 5a) shows the Zr $3d_{5/2}$ peak at 184.12 eV and the Zr $3d_{3/2}$ peak at 181.65 eV, matching previously reported values for ZrO_2 [26] and confirming its presence. The O 1s spectrum (Fig. 5b) can be fitted with two components: the higher-binding-energy peak at 531.72 eV corresponds to surface oxygen vacancies, while the lower-binding-energy peak at 529.42 eV arises from lattice oxygen in the Ag-doped ZrO_2 nanoparticles. The change in peak intensity reflects variations in the number and concentration of oxygen vacancies [27]. In the Ag 3d spectrum (Fig. 5c), the peaks at 368.51 eV (Ag $3d_{5/2}$) and 374.81 eV (Ag $3d_{3/2}$) correspond to metallic Ag^0 and Ag^+ ions, respectively, consistent with earlier reports [28]. These XPS results, together with the EDX and XRD data, confirm the successful synthesis of pure ZrO_2 and Ag-doped ZrO_2 nanoparticles.

REDVET - Revista electrónica de Veterinaria - ISSN 1695-7504
Vol 25, No. 2 (2024)
http://www.veterinaria.org
Article Recieved: 16/09/2024, Revised: 18/10/2024, Accepted: 09/12/2024

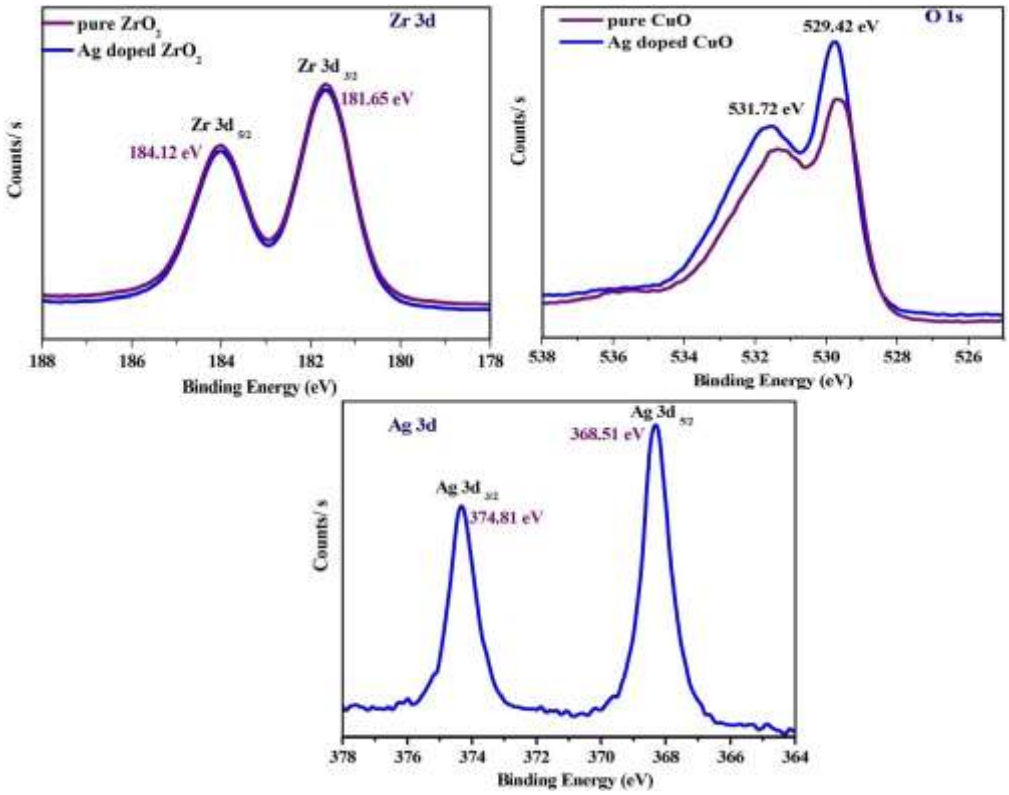

Fig. 5XPS spectrum of Zr 3d,O 1s and Ag 3d

3.4 UV-visible spectra

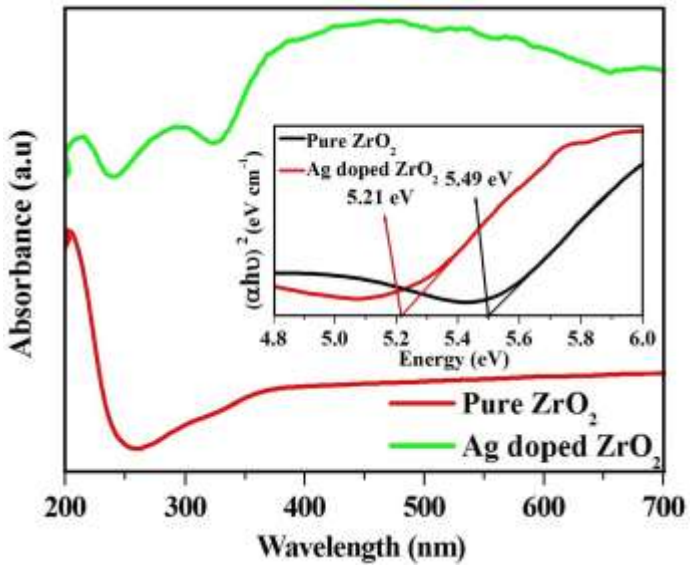

Fig. 6 UV-visible absorbance spectra of pure ZrO_2 and Ag doped ZrO_2 nanoparticles.

The UV-visible absorption spectra of pure ZrO_2 and Ag-doped ZrO_2 nanoparticles are shown in Fig. 6. The optical response of such nanostructures is governed by the absorbance associated with charge transitions from the valence band to the conduction band [29]. Broad absorption arises from surface-related defects created in the particles [30]. The band-gap energy was determined from a Tauc plot by extrapolating the linear portion of $(\alpha h\nu)^2$ versus photon energy ($h\nu$) to the energy axis (inset of Fig. 6). The relationship for allowed direct transitions follows the Tauc equation [31]:

$$\alpha h\nu = C(h\nu - Eg)^n \quad \text{---------- (5)}$$

where 'C' is a constant, 'h' is Planck's constant, 'ν' is the frequency, and 'Eg' is the band-gap energy; the exponent 1/2 applies to a direct-band-gap semiconductor. The absorption edge of Ag-doped ZrO_2 shifts to longer wavelengths compared with pure ZrO_2, confirming successful Ag incorporation into the ZrO_2 lattice. The Ag-doped sample exhibits strong absorption across both UV and visible regions, whereas pure ZrO_2 shows weak visible absorption and its transmittance rises to near-100 %. The measured band-gap energies are 5.49 eV for pure ZrO_2 and 5.21 eV for

REDVET - Revista electrónica de Veterinaria - ISSN 1695-7504
Vol 25, No. 2 (2024)
http://www.veterinaria.org
Article Recieved: 16/09/2024, Revised: 18/10/2024, Accepted: 09/12/2024

Ag-doped ZrO_2. This reduction is attributed to a shift of the Fermi level toward the conduction band caused by the increased carrier concentration introduced by Ag doping [32].

3.5 PL spectra

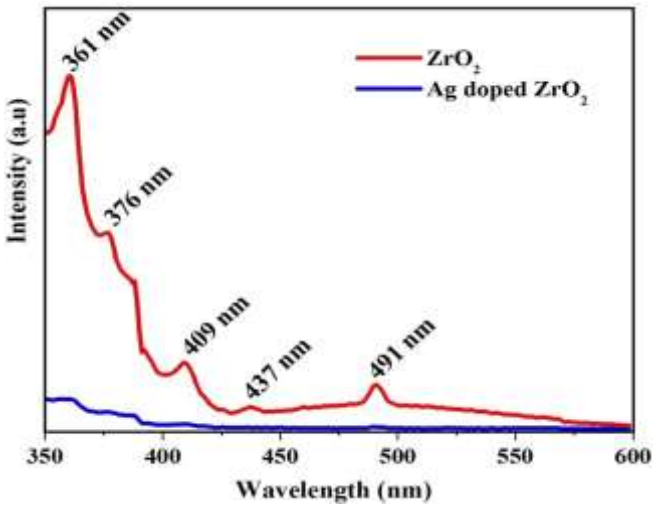

Fig. 7 PL spectra of pure ZrO_2 and Ag doped ZrO_2 nanoparticles.

The room-temperature photoluminescence (PL) spectra of pure ZrO_2 and Ag-doped ZrO_2 nanoparticles are presented in Fig. 7. The figure shows that Ag doping reduces the electron-hole recombination rate, resulting in lower emission intensity for the Ag-doped sample. Both samples display a broad UV band from ≈ 300 nm to ≈ 400 nm, while pure ZrO_2 exhibits three additional visible-region peaks. The strong UV band is split into two peaks at ≈ 360 nm and ≈ 376 nm, which arise from near-band-edge emission (NBE) of free excitons in the conduction band [33]. A violet emission at ≈ 409 nm originates from interstitial zirconium ions; radiative recombination between the shallow donor (Zr_i) and deep acceptor (V_o) levels produces this violet signal [34]. Blue emissions at ≈ 437 nm and ≈ 491 nm are attributed to defect-related transitions or surface impurities—such as intrinsic defects, oxygen vacancies, surface states, or interstitial metal ions—formed during crystal growth [25].

3.6 Anticancer activity

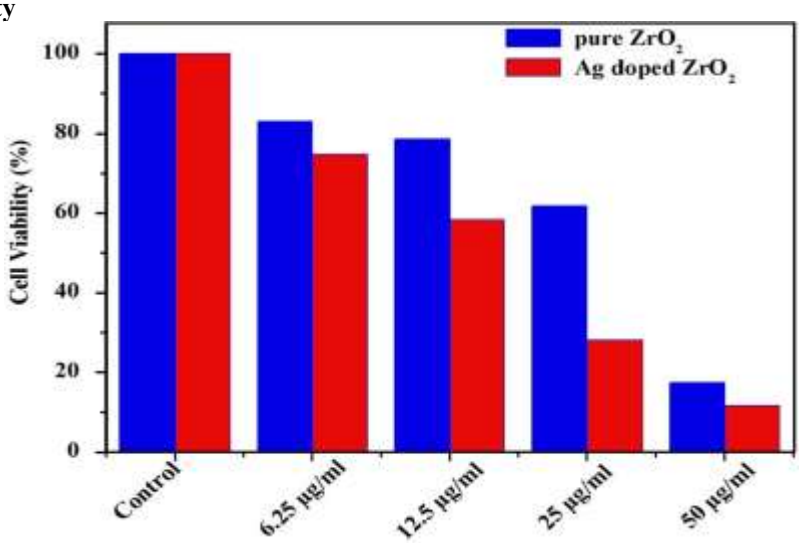

Fig. 8 % cell viability values of AGS cells treated by different concentrations/ doses of pure ZrO_2 and Ag doped ZrO_2 nanoparticlesafter the incubation period of 24hrs by MTT assay.

The anticancer potential of green-synthesized pure ZrO_2 and Ag-doped ZrO_2 nanoparticles was assessed against AGS human gastric adenocarcinoma cells using the MTT assay over a concentration range of 6.25–100 µg ml^{-1}. Figure 8 shows the relative percent viability of the cancer cells. Both nanoparticle types strongly inhibited AGS growth, with the highest inhibition observed at 100 µg ml^{-1}. Pure ZrO_2 reduced viability from 84.51 % (6.25 µg ml^{-1}) to 18.32 % (100 µg ml^{-1}), while Ag-doped ZrO_2 caused a decline from 78.69 % (6.25 µg ml^{-1}) to 11.92 % (100 µg ml^{-1}). These results demonstrate that Ag-doped ZrO_2 nanoparticles exhibit greater anticancer activity than pure ZrO_2. Cytotoxicity of

REDVET - Revista electrónica de Veterinaria - ISSN 1695-7504
Vol 25, No. 2 (2024)
http://www.veterinaria.org
Article Recieved: 16/09/2024, Revised: 18/10/2024, Accepted: 09/12/2024

ZrO_2 is generally linked to several factors such as particle size, ROS generation, and release of metal ions [35]. Researchers have reported that ZrO_2 nanoparticles can cause genotoxic effects, oxidative stress, cell death, DNA damage, and inflammatory responses [36]. In this study, Ag-doped ZrO_2 nanoparticles induced intracellular ROS in a dose-dependent manner, and the viability of AGS cells decreased accordingly. The nanoparticles disrupt the cell membrane and impair cancer-cell function. Zinc oxide nanoparticles are known to be cytotoxic toward rapidly proliferating cells because they boost ROS production; the prepared nanoparticles act as a redox system inside cancer cells, generating high levels of ROS that trigger oxidative stress. This leads to biomolecular damage (lipid peroxidation, protein denaturation), necrosis, DNA damage, and ultimately apoptotic cell death [37]. Silver ions promote apoptosis in malignant cells by raising the concentration of free radicals [38, 39]. The reduced optical band gap of Ag-doped ZrO_2 plays a critical role in ROS-mediated cytotoxicity. Moreover, the Clerodendrum infortunatum leaf-extract-mediated Ag-doped nanoparticles showed stronger cytotoxic effects than pure ZrO_2, highlighting the impact of silver ions in enhancing cytotoxicity.

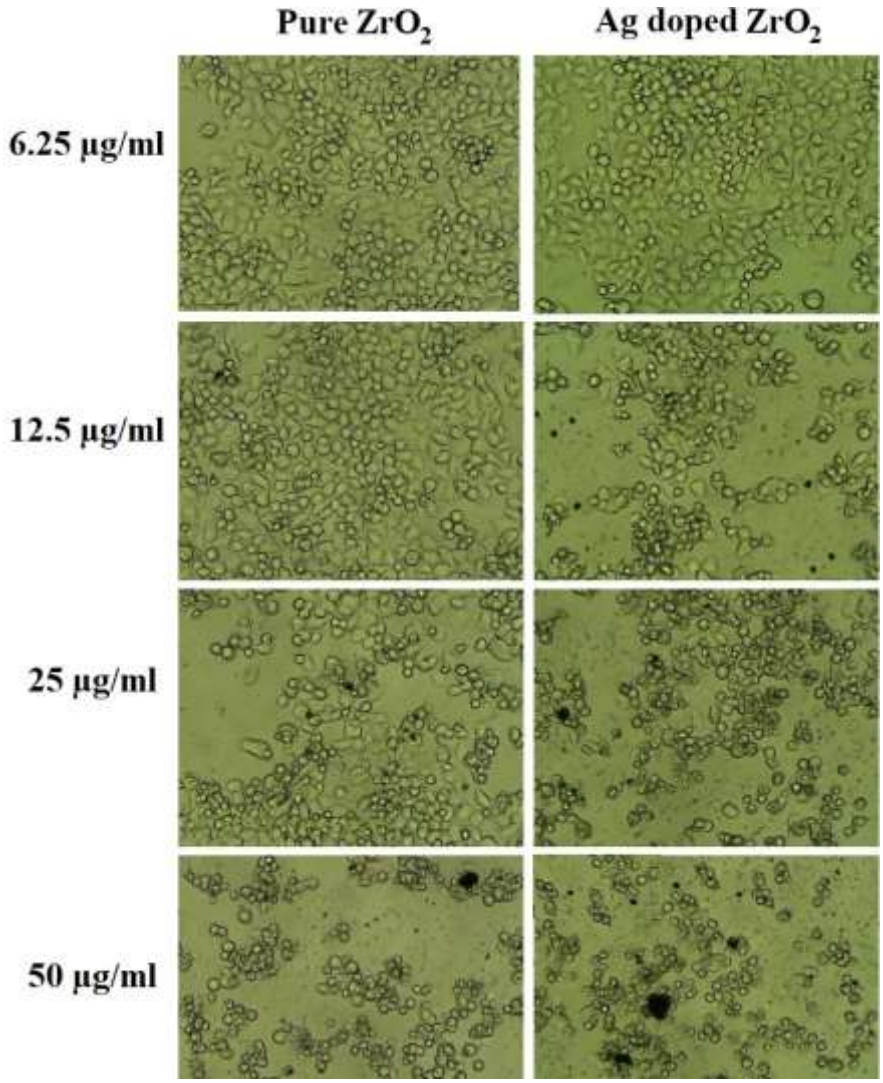

Fig. 9 Cell numbers and viability evaluated using MTT staining after 24 h seeding. (6.25 µg/ml, 12.5 µg/ml, 25 µg/ml, 50 µg/ml and 100 µg/ml)

The present work examined the growth-inhibitory effect of pure ZrO_2 and Ag-doped ZrO_2 nanoparticles on human AGS cells using the MTT assay. Figure 9 shows the cell-viability results: both samples suppressed AGS proliferation, and increasing concentrations ($6.25, 12.5, 25, 50, 100\ \mu g\ ml^{-1}$) led to a progressive decline in survival rates, indicating substantial cell death after treatment [40]. Rajendran et al. [41] reported that nanoparticle treatment significantly reduced cell-viability percentages in a concentration-dependent manner. Green-synthesized nanoparticles intended for imaging or drug delivery are often coated with bioconjugates (DNA, proteins, monoclonal antibodies) to target specific cells. Because these coatings are designed to interact with cells, it is essential to verify that they do not introduce adverse effects—especially whether naked or coated particles undergo biodegradation inside the cellular environment and what cellular responses the degraded material may provoke [42]. The MTT data show that Ag-doped ZrO_2 nanoparticles

caused more cell death than pure ZrO_2, suggesting a higher cytotoxic potential. Consequently, the Clerodendrum infortunatum leaf-extract-mediated synthesis of Ag-doped ZrO_2 indicates that these particles could exert chemotherapeutic effects and serve as a foundation for future drug development.

Conclusion

The comprehensive characterization and biological evaluation of pure ZrO_2 and Ag-doped ZrO_2 nanoparticles demonstrate that Ag incorporation significantly modifies structural, optical, and anticancer properties. XRD, TEM, and XPS analyses confirm the formation of a face-centered cubic ZrO_2 lattice with reduced crystallite size, increased strain, and lower dislocation density upon Ag doping. HR-TEM and SAED reveal well-defined (101) lattice planes, while EDS and XPS verify the presence of metallic Ag^0 and Ag^+ species. UV-visible spectroscopy shows a red-shifted absorption edge and a narrowed band gap (5.49 eV → 5.21 eV), indicating successful Ag integration. Photoluminescence spectra exhibit diminished emission intensity due to suppressed electron–hole recombination. In vitro MTT assays against AGS gastric adenocarcinoma cells reveal dose-dependent cytotoxicity, with Ag-doped ZrO_2 achieving a lower cell viability (≈ 12 % at 100 µg ml^{-1}) than pure ZrO_2 (≈ 18 %). The enhanced anticancer activity is attributed to increased ROS generation, reduced band gap, and the release of Ag^+ ions, which trigger oxidative stress, membrane damage, and apoptotic pathways. MTT results further confirm a concentration-dependent decline in AGS survival, underscoring the potential of Clerodendrum infortunatum leaf-extract-mediated Ag-doped ZrO_2 as a promising chemotherapeutic agent warranting further in vivo investigation.

Reference

1. P. C. Mane, D. D. Kadam, A. N. Khadse, Green adeptness in synthesis of non-toxic copper and cobalt oxide nanocomposites with multifaceted bioactivities, Cancer Nanotechnology, 14 (2023).
2. P.Jakinala, H.N. Lavudi, N. Angali, S. Ganderla, K.K. Inampudi, S.B. Andugulapati,M. Srinivas and M.R. Katika, Green synthesis of ZnO-Ag nanocomposite using Stenotaphrumsecundatum grass extract: Antibacterial activity and anticancer effect in oral squamous cell carcinoma CAL 27 cells, Inorganic Chemistry Communications, 152 (2023) 110735-110741.
3. D.R.A. Preethi, S. Prabhu, V. Ravikumar and A. Philominal, Anticancer activity of pure and silver doped copper oxide nanoparticles against A549 Cell line, Materials Today Communication, 33 (2022) 104462-104467.
4. R. G. Chaudhary, A. K. Potbhare, P. B. Chouke, and A. R. Rai, Graphene-based materials and their nanocomposites with metal oxides: biosynthesis, electrochemical, photocatalytic and antimicrobial applications, Materials Research Foundations, 83 (2020) 79–116.
5. X. Qu, D. Zhou, J. Lu, D. Qin, J. Zhou, and H.-J. Liu, Cancer nanomedicine in preoperative therapeutics: nanotechnologyenabled neoadjuvant chemotherapy, radiotherapy, immunotherapy, and phototherapy, Bioactive Materials, 24 (2023) 136–152.
6. S. Dubey, T. Virmani, S. K. Yadav, A. Sharma, G. Kumar and A. Alhalmi, Breaking Barriers in Eco-Friendly Synthesis of Plant-Mediated Metal/Metal Oxide/Bimetallic Nanoparticles: Antibacterial, Anticancer, Mechanism Elucidation, and Versatile Utilizations, Journal of Nanomaterials, 2024 (2024).
7. S. Balaji, B.K. Mandal, S. Ranjan, N. Dasgupta and R. Chidambaram, Nano-zirconia – Evaluation of its antioxidant and anticancer activity, Journal of Photochemistry and Photobiology B: Biology, 170 (2017) 125-131.
8. S. Alanazi, Z. M. Alaizeri, R. Lateef, N. Madkhali, A. Alharbi and M. Ahamed, Zn Doping Improves the Anticancer Efficacy of SnO_2 Nanoparticles, Applied Sciencese, 13 (2023) 12456-12462.
9. Y. Mbenga, J.O. Adeyemi, D.M.N. Mthiyane, M. Singh and D.C. Onwudiwe, Green synthesis, antioxidant and anticancer activities of TiO2 nanoparticles using aqueous extract of Tulbhagia violacea, Results in Chemistry, 6 (2023) 101007-101012.
10. A. Fakhri, S. Behrouz, I. Tyagi, S. Agarwal and V. K. Gupta, Synthesis and characterization of ZrO_2 and carbon-doped ZrO_2 nanoparticles for photocatalytic application, Journal of Molecular Liquids, 216 (2016) 342-346.
11. A. Annu, C. Sivasankari and U. Krupasankar, Synthesis and characerization of Zro2 nanoparticle by leaf extract bioreduction process for its biological studies. Mater Today Procceding, 33 (2020) 5317–5323.
12. C. Dhandapani, R. Narayanasamy and S. N. Karthick, Drastic photocatalytic degradation of methylene blue dye by neodymium doped zirconium oxide as photocatalyst under visible light irradiation, Optik, 127 (2016) 10288–10296.
13. T. V. Tran, D. T. C. Nguyen, P. S. Kumar, A. T. M. Din, A. A. Jalil and D. V. N. Vo, Green synthesis of ZrO2 nanoparticles and nanocomposites for biomedical and environmental applications: a review, Environmental Chemistry Letters, 20 (2022) 1309–1331.
14. S. Raj, M. Hattori and M. Ozawa, Ag-doped ZrO2 nanoparticles prepared by hydrothermal method for efficient diesel soot oxidation, Materials Letters, 234 (2019) 205–207.
15. K. Parveen, V. Banse and L. Ledwani, Green synthesis of nanoparticles: Their advantages and disadvantages, American institute of Physics, 1724 (2016) 020048-20053.
16. F. Ameen, Optimization of the synthesis of fungus-mediated bi-metallic Ag-Cu nanoparticles, Applied Science, 12 (2022) 1384-1387.

17. R. Singh and S. Dutta, Synthesis and characterization of solar photoactive TiO_2 nanoparticles with enhanced structural and optical properties, Advanved Powder Technology, 29 (2017) 211-218.
18. S. Kumar, N. Bithel, S. Kumar, Kishan, M. Sen and C. Banerjee, Phyto-mediated synthesis of zinc oxide nanoparticles from Clerodendrum infortunatum L. leaf extract and evaluation of antibacterial potential, South African Journal of Botany, 164 (2024) 146-151.
19. R. Kaliyaperumal, K. Nagaraj, V. K. Poovan, K. Sakthikumar, C. Govindasamy and A. S. Sivakumar, Hydrothermal implementation with Zirconia: synthesis, characterization and investigation of biocidal activity of Ag/ZrO2 nanocomposites, Zeitschrift für Physikalische Chemie, 238 (2023).
20. S. K. Pradhan, V. Pareek, J. Panwar and S. Gupta, Synthesis and characterization of ecofriendly silver nanoparticles combined with yttrium oxide (Ag-Y2O3) nanocomposite with assorted adsorption capacity for Cu(II) and Cr(VI) removal: A mechanism perspective, Journal of Water Process Engineering, 32 (2019) 100917-100932.
21. J. Samuel, J. E. shaji, S. S. J. Dhas, S. Suresh, V. S. Vinita and C.S.Biju, UV-blocking performance and antibacterial activity of Cd, Ba co-doped ZnO nanomaterials prepared by a facile wet chemical method, Surface and Interface Analysis, 1 (2023) 1-14.
22. C. J. C. Singh, J. Samuel, C. S. Biju, S. S. J. Dhas and S. Usharani, Effect of Sn doping on the structural, photoluminescence, ultraviolet fltering and antibacterial activity of ZnO nanorods, Optical and Quantum Electronics, 55 (2023) 1072-1093.
23. R. Yogamalar, R. Srinivasan, A. Vinu, K. Ariga and A.C. Bose, X-ray peak broadening analysis in ZnO nanoparticles, solid State Communication, 149 (2009) 1919-1923.
24. H. M. Shinde, S. V. Kite, B. S. Shirke and K. M. Garadkar, Eco-friendly synthesis of Ag-ZrO2 nanocomposites for degradation of methylene blue, Journal of Mater Science: Materials in Electronics, 32 (2021) 14235–14247.
25. J. Samuel, T.S. F. Rajesh, C.S. Biju, S. S. J. Dhas and S. Usharani, Synthesis, structural, photoluminescence, ultraviolet blocking and antibacterial performances of Ba-doped ZnO nanostructures, Results in Optics, 12 (2023) 100482-100489.
26. A. Bumajdad, A. A. Nazeer, F. A. Sagheer, S. Nahar and M. I. Zaki, Controlled Synthesis of ZrO2 Nanoparticles with Tailored Size, Morphology and Crystal Phases via Organic/Inorganic Hybrid Films, Scientific Report, 8 (2018) 3695-3704.
27. J. Samuel, S. Suresh, S. Shabna, V. S. Vinita, N. J. Ananth, P. M. S. Shinu, A. Mariappan, T. Simon, Y. Samson and C.S. Biju, Characterization and antibacterial activity of Ti doped ZnO nanorods prepared by hydrazine assisted wet chemical route, Physica E Low Dimensions System and Nanostructures, 143 (2022) 115374-115381.
28. S. Iqbal, M. Javed, A. Bahadur, M.A. Qamar, M. Ahmad, M. Shoaib, M. Raheel, N. Ahmad, M.B. Akbar and H. Li, Controlled synthesis of Ag-doped CuO nanoparticles as a core with poly(acrylic acid) microgel shell for efcient removal of methylene blue under visible light, Journal of Materials Science: Materials in Electronics, 31 (2020) 8423-8432.
29. J. Fanga and Y. Xuan, Investigation of optical absorption and photothermal conversion characteristics of binary CuO/ZnO nanofluids, RSC Advances, 7 (2017) 56023-56028.
30. H, Huang, X. Sun, S. Wang, Y. Liu, X. Li, J. Liu, Z. Kang and S. T. Lee, Strong red emission of pure Y_2O_3nanoparticles from oxygen related defects, Dalton Transactions, 40 (2011) 11362-11366.
31. M. Mohammadikish and A.A. Akradi, Synthesis and optical band gap determination of CuO nanoparticles from salen-based infinite coordination polymer nanospheres, Material Research Express, 6 (2019) 045013.
32. J. Samuel, J. E. shaji, S. S. J. Dhas, S. Suresh, V. S. Vinita and C.S.Biju, UV-blocking performance and antibacterial activity of Cd, Ba co-doped ZnO nanomaterials prepared by a facile wet chemical method, Surface and Interface Analysis, 1 (2023) 1-5.
33. A. Ravi, J. Samuel, S. S. J. Dhas, S. Usharani, T. Simon, D. S. Kumar, S. K. J. Vijitha, A. Sivakumar, R. S. Kumar, C. S. Biju, Structural, morphological, optical and antibacterial performances of rare earth (Sm)-doped ZnO nanorods, Journal of Rare Earths, (2024) In press.
34. A. Pramothkumar, N. Senthilkumar, K.C.M. Gnana Malar, M. Meena and I.V. Potheher, A comparative analysis on the dye degradation efciency of pure, Co, Ni and Mn-doped CuO nanoparticles, Journal of Materials Science: Materials in Electronics, 30 (2019) 19043-19047.
35. S. Balaji, B. K. Mandal, S. Ranjan, N. Dasgupta and R. Chidambaram, Nano-zirconia – Evaluation of its antioxidant and anticancer activity, Journal of Photochemistry and Photobiology B: Biology, 170 (2017) 125-133.
36. A. K. Chitoria, A. Mir and M.A. Shah, A review of ZrO2 nanoparticles applications and recent advancements, Ceramics International, 49 (2023) 32343-32358.
37. S. Prabhu, T.D. Thangadurai, P.V. Bharathy, Greenbased Biosynthesis of Zinc Oxide Nanoparticles Using Clitoriaternatea Flower Extract and Its Antibacterial Activity, Nano Biomedical Engineering, (2021) 394-400.
38. M. E. T. Yazdi, M. S. Amiri, S. Akbari, M. Sharifalhoseini, F. Nourbakhsh, M. Mashreghi, M. R. E. Yousefi, M. Abbasi, A. H. Modarres, Green synthesis of silver nanoparticles using helichrysum graveolens for biomedical applications and wastewater treatment, Bio. NanoScience, 10 (2020) 1121–1127.

39. M. J. Akhtar, H.A. Alhadlaq, A. Alshamsan, M.A. Majeed Khan and M. Ahamed, Aluminum doping tunes band gap energy level as well as oxidative stress-mediated cytotoxicity of ZnO nanoparticles in MCF-7 cells, Scientific Reports, 5 (2015) 13876.
40. M. Ahamed, M. J. Akhtar, M. A. M. Khan and H. A. Alhadlaq, Enhanced Anticancer Performance of Eco-Friendly-Prepared MoZnO/RGO Nanocomposites: Role of Oxidative Stress and Apoptosis, ACS Omega, 7 (2022) 7103.
41. R. Rajendran and A. Mani, Photocatalytic, antibacterial and anticancer activity of silver-doped zinc oxide nanoparticles, Journal of Saudi Chemical Society, 24 (2020) 1010–1024.
42. N. Lewinski, V. Colvin and R. Drezek, Cytotoxicity of Nanoparticles, small, 4 (2008) 26–49.